Biophys J BioFAST, published on April 29, 2005 as doi:10.1529/biophysj.105.060608

Interhead distance measurements in myosin VI via SHRImP support a simplified hand-over-hand model

Hamza Balci[1], Taekjip Ha[1], H. Lee Sweeney[2], Paul R. Selvin[1*]

[1]Physics and Biophysics Depts. Department, University of Illinois, Urbana-Champaign, and [2]University of Pennsylvania, Penn. Muscle Institute.

*To whom correspondence should be addressed:

Loomis Lab of Physics

1110 W. Green St.

Univ. of Illinois

Urbana, IL 61801

selvin@uiuc.edu

(217) 244-3371 (tel); (217) 244-7187 (fax)

Myosin-VI walks in a hand-over-hand fashion with an average step size of 30 nm, which is much larger than its 10 nm lever arm. Recent experiments suggest that myosin VI structure has an unfolded and flexible region in the proximal tail which makes such a large step possible. In addition, cryo-EM images of actomyosin-VI show the two heads bound to the actin monomers with a broad distribution of distances, including some as close as a few nanometers. This observation when combined with the existence of a flexible region in the structure, which takes part in stepping, challenged the hand-over-hand model. In the hand-over-hand model the lever arm is considered to be rigid and the inter-head separation should not be very different from 30 nm. We considered an alternative model in which myosin-VI heads sequentially take 60 nm steps while the inter-head separation alternates between a large and small value (x and 60-x, where $x<30$). In order to clarify these issues, we used a new technique, SHRImP, to measure the inter-head distance of nearly rigor myosin-VI molecules. Our data shows a single peak at 29.3 ± 0.7 nm, in agreement with the straightforward hand-over-hand model.

Myosin VI, similar to the other 17 members of the myosin superfamily (1), has three domains in its structure: a motor domain (N terminal) that binds to actin and shows ATPase activity, a neck domain that binds light chains or calmodulin, and a tail domain (C terminal) that binds to cargo. It was first discovered in Drosophila (2), and later was identified in many higher organisms ranging from Caenorhabditis elegans to humans (3-5). The gene for myosin VI is defective in the deaf mouse, Snell's Waltzer, suggesting that myosin VI is involved in the function of sensory hair cells (5,6). Myosin VI is unique in the myosin family in that it is the only member of the family that walks towards the pointed (-) end of actin (7). It is also observed that myosin VI colocalizes with clathrin coated pits (8), which when combined with its directionality, suggests that it is involved in endocytosis (9).

Recently myosin VI has attracted attention due to two of its unusual properties - processivity and step-size. Biochemical characterization and electron microscopy studies on myosin VI have shown that expressed full-length myosin VI is a monomer and is a non-processive motor (10). However, it has also been shown that dimerized myosin VI can take many steps before detaching from actin (11-14), and hence acts as a processive motor. It is not clear at this point how myosin VI functions within the cell: as a monomer, a dimer, or both. However, extensive optical trap experiments on myosin VI imply a possible explanation by attributing multi funtionality, which might reguire both monomers and dimers of this motor (15). The molecules that we use in this study are dimerized constructs of myosin VI. The second unusual property of myosin VI, which is the topic of this article, was realized when motility experiments on dimerized constructs of myosin VI measured a

step size that is not compatible with the assumed structure of this motor using the well established lever arm mechanism (11-14).

Hand-over-hand model of walking using a lever arm mechanism has been well established for processive motors in the myosin and kinesin families (16-24). The step of these molecular motors consists of two parts: a power stroke and a diffusive search that follows the power stroke (22). The size of the power stroke is comparable to the size of the light chain domain which acts as the lever arm. For example for myosin V, the step is formed from a ~23 nm (size of the light chain domain) power stroke and a ~12 nm diffusive search (22). However, in the case of myosin VI the situation is quite different since the light chain domain (~10 nm) is much shorter than the measured step size (~30 nm) (13,14). Two possible scenarios were considered: there is a rigid extension to the lever arm which would enable a longer power stroke, or there is a flexible compliant region which enables the motor to go through a longer diffusive search. Several experimental observations (13,25) favor the proximal tail to act as a flexible compliant region rather than a rigid extension to the lever arm. The emerging picture is that, after the power stroke of the motor (~12 nm), the head domain goes through a biased diffusive search on the actin monomer (~20 nm) until it finds the next binding site.

The complications in myosin VI motility were further increased with cryo-electron microscopy images of myosin VI. These images showed that for some of the motors, the two heads of the dimer were bound to adjacent actin monomers with a separation much less than 30 nm (12). These images, when considered with the additional degree of freedom

provided by the flexible region in the proximal tail domain, challenged the hand-over-hand model of walking. Fig. 1b shows an alternative model where the heads alternately take 60 nm steps and the distance between the heads is either x nm or 60-x nm, depending on which head took the last step, where x could have any value between ~5 nm (since the two heads can not be on the same actin monomer) and 30 nm (see Fig.1-b). This model will be referred to as asymmetric hand-over-hand model in the rest of the manuscript. In order to clarify this issue we measured the separation between the myosin VI heads, rather than the step size. In the hand-over-hand model, we would expect the inter-head separation to show a single peak at 30 nm, whereas the asymmetric hand-over-hand model should show two peaks: one at x nm and another at 60-x nm. We used our recently introduced Single-molecule High Resolution Imaging with Photobleaching (SHRImP) to determine the distance between eGFP molecules on the heads of myosin VI with nanometer precision (26,27).

Materials and Methods

Imaging. Olympus (Melville, NY) IX-71 microscope, Olympus Apo 100×, 1.65 NA oil objective, and high refractive index cover slips (also from Olympus) were used in the objective type TIR setup. The eGFP molecules were excited using Melles Griot (Carlsbad, CA) ion laser at 488 nm wavelength. Images were captured by using a slow-scan back-thinned Andor (South Windsor, CT) CCD camera, allowing continuous imaging with no interframe dead time. The image capture frequency was 2 Hz (13).

Sample preparation.

The samples were prepared as described in (13). The sapphire cover slips and glass slides were sonicated in acetone for 20 minutes, rinsed with doubly deionized water, sonicated in 1 M KOH for another 20 minutes, and finally rinsed again with doubly deionized water. The sample chamber was prepared by flowing 10 mM BSA-biotin, waiting for 10 min, washing with M5BufBH (20 mM HEPES pH 7.6, 2 mM MgCl2, 25 mM KCl, 1 mM EGTA), followed by 0.5 mg/ml streptavidin, waiting for 5 min, followed by 0.2 μM 1:10 biotinylated/unbiotinylated phalloidin-stabilized F-actin, followed by M5+ (M5BufBH plus 10 mM DTT and 100 mg/ml calmodulin) wash, followed by myosin VI sample solution. Myosin VI sample solution consists of 50 pM eGFP-myosin VI, 100 mM DTT, 100 mg/ml calmodulin, and 1–2 μM ATP, in M5BufBH.

Data Analysis

We have used SHRImP (26) to measure the distance between the myosin VI heads in the presence of very low concentration of ATP. SHRImP takes advantage of quantal photobleaching of fluorescent molecules to resolve two fluorophores which lie on the same plane and which have overlapping point spread functions (PSF). In this case, there would be a two-step photobleaching event, and each of the steps corresponds to the photobleaching of one of the dyes. The images both before and after photobleaching of one of the dyes are fit to two dimensional Gaussian functions. The image after one of the dyes photobleaches is used to determine the PSF of one of the dyes and the difference between this image and the one before the first photobleaching is used to determine the PSF of the other dye. Hence, both dyes can be simultaneously localized by using this simple idea.

Results and Discussion

We used SHRImP to measure the distance between the myosin VI heads. The fluorophores are two enhanced green fluorescent proteins (eGFP), located at the N-terminus, or head region, of the myosin VI dimer. The data is taken in the presence of very low concentration of ATP in order to make sure the myosin heads are bound to the actins in a configuration relevant for stepping (1 μM which is about 3 % of that used for motility experiments). However, the concentration of ATP is low enough that almost all of the dyes are stationary. Among the thousands of molecules we imaged in the course of this study, we noticed only a few which moved 1-2 steps. These were not included in the analysis. This is a necessary condition in order to be able to measure the separation between the two heads accurately and avoid any confusion that could result from the moving of one or both heads during the measurement. Since the myosin molecules do not move, it is important to make sure that they land on actins rather than non-specifically bind to the surface. In order to test if any non-specific binding occurs, the actins were decorated with a high concentration of myosin VI molecules. We include an image of the actin filaments decorated with myosin VI molecules as Supplementary Online Material. This image clearly shows that the myosin molecules bind only to the actins and not to the surface. In addition, the actin concentration is low enough and the length of the actin where multiple actins cross-over is far shorter than the full-length of the actin filaments to assure us that a myosin VI molecule would bind to only one actin filament.

Fig. 2a shows an example of two-step photobleaching. The intensity on the y-axis corresponds to the maximum of the PSF although the same two-step photobleaching can be

observed in the total integrated area under the PSF as well. Fig. 2b shows the corresponding PSF's before and after photobleaching. The difference between the first two graphs is shown in the third graph, which is the PSF of the eGFP that photobleached first. The details of the data analysis using SHRImP are given in Ref. (26).

The frequency of the two-step photobleaching events was sensitively dependent on the experimental conditions used in preparing the sample. However, 1-2 % was the typical frequency that showed clear two-step photobleaching. In the best cases, this frequency was as high as 5%. Most of the dyes showed a single step photobleaching. It is not clear at this point why higher frequency of two-step photobleaching could not be observed, since in gel filtration experiments our samples showed a single band of doubly-labeled myosin VI (data not shown). However, there are several reasons which would reduce the frequency of observing clear two-step photobleaching events. The relatively long integration time we use in acquiring the images is one of these reasons. The images were taken every 0.5 seconds, therefore if the dyes photobleached one after another within 1-2 seconds, we would not be able to clearly distinguish this event from a single step photobleaching event. In addition, it is possible that one of the dyes photobleached within the first 1-2 seconds after the laser is turned on. This case would not be counted as a two-step photobleaching event since the time is too short to get reliable statistics. In a few rare cases we observed broad, rather than single step, photobleaching events which indicates that the myosins formed aggregates. We submit an image as Supplementary Online Material showing the concentration of myosin VI molecules we used in the experiments. As is clear in this image, the concentration of myosin VI molecules is low enough to image single molecules.

Fig. 3 shows a histogram of the separation between the myosin VI heads determined from the two-step photobleaching events and various fits made to this histogram. There are 96 points in the histogram. The average inter-head separation of the 96 molecules is 31.0 nm, and the standard deviation is 15.4 nm. Each point reflects an average distance determined from the best Gaussian fits to several pre-and post-photobleach events. Typically 4 frames were used to compute the average distance. However, in some cases only 2 frames yielded good enough fits that could be used, and in some cases as many as 9 frames were used to find the average distance. The center of a Gaussian for each frame was typically determined within an error of 5-6 nm. The best resolution (in localizing the center of the Gaussian) obtained was 3 nm, and the minimum acceptable resolution (to be included in the histogram) was 10 nm.

The curves in Fig. 3 are three different fits to the data. Different fits were used in order to model the alternative walking styles presented in Fig. 1. In the case of symmetric hand-over-hand model, we would expect the interhead separation to peak at 30 nm, and hence a single Gaussian should be able to represent the histogram. A Gaussian fit of the form $y=y_0+a\ \exp[-0.5*([x-x(0)]/b)^2]$ to the histogram results in $x(0) = 29.2 \pm 0.8$ nm, which is in very good agreement with the symmetric hand-over-hand model. The other parameters generated by the fit are $y_0=0.9 \pm 0.6$ nm, $a= 19.9\pm1.4$, and $b=9.7\pm0.9$ nm. The full-width at half maximum of the Gaussian is 23.8 nm. However, the broadness of the peak we observe in the histogram and in the corresponding Gaussian fit suggests that two closely spaced Gaussians may be able to describe the data as well. In order to study this possibility further,

we fit the data with a function of the form $y=y_0+a\ \exp[-0.5*([x-x_1(0)]/b)^2] + c\ \exp[-0.5*([x-x_2(0)]/d)^2]$. This fit is shown as the black curve in Fig.2, and the corresponding parameters are y_0=0.9 ± 0.3 nm, a=21.7±0.9, $x_1(0)$=27.3±0.5 nm, b=7.2±0.5 nm, c=8.2±1.3, $x_2(0)$=43.9±1.0 nm, and d=4.2±0.7 nm. This function corresponds to a model in which the separation between the heads alternate between 27.3 nm and 43.9 nm. This would suggest that even if the asymmetry between the interhead separations is as large as 43.9-27.3=16.6 nm we would not be able to distinguish it from the symmetric case presented earlier. Even though the data seems to be very well described by such a fitting function (Reduced χ^2 = 1.0), the amplitudes of the Gaussians which is a measure of the frequency of observing the corresponding interhead separation do not represent the experimental conditions we used. The amplitude of the Gaussian for 27.3 nm interhead separation is 21.7 and the amplitude for 43.9 nm separation is 8.2, which means that 73 % of the time we observe the myosins when the interhead separation is 27.3 nm. However, there is no reason for such a strong bias in the statistics to happen towards one of the interhead separation, and on average we should observe the two interhead separations with equal frequency. Another problem with this fit is that 27.3 nm and 43.9 nm result in a step size of 35.6 nm, which is significantly larger than the expected 30 nm step. A more realistic fit which consists of two Gaussians would be one in which the amplitudes of the Gaussians are equal to each other (a=c in the previous function), and the sum of the two separations equals 60 nm (the red curve in Fig.3). Such a fit, $y=y_0+a\ \exp[-0.5*([x-x_1(0)]/b)^2] + a\ \exp[-0.5*([x-(60-x_1(0))]/d)^2]$, is shown as the red line in Fig. 2. The parameters of the function are determined to be y_0=0.6 ± 0.5 nm, a= 12.0±0.8, $x_1(0)$=34.3±0.9 nm, b=11.6±1.6 nm, and d=5.5±0.7 nm, and the reduced χ^2 = 1.5. According to this fit, the peaks of the Gaussians are at 34.3 nm and 25.7

nm which result in an asymmetry of 8.6 nm. Hence, the resolution of our data in separating two peaks from one would be somewhere between 8.6 nm and 16.6 nm. A non-rigorous and conservative estimate for resolution would be 14 nm.

Conclusion

Our results are the first application of SHRImP on motor proteins, and they represent the unique capabilities of this technique in measuring distances between 10 nm to 100 nm. We show that in the presence of very low concentration of ATP the separation between the heads of myosin VI is 29.3 ± 0.7 nm, in agreement with the straightforward hand-over-hand model. Although the distribution in the measured head-to-head separation does not allow us to rule out a small asymmetry, we can set an upper limit of 14 nm for this asymmetry in the interhead separation (i.e. the interhead separation can not be more asymmetric than $x_1(0)$=23 nm and $x_1(0)$=37 nm). Since such large separations between the heads are structurally not possible by considering only the light chain domains (the maximum possible separation a 10 nm long lever arm can provide is 10+10=20 nm), the flexible region which enables the 60 nm step should also be at least partially open in between steps as well.

We thank Matthew Gordon for sharing his SHRImP software with us, and Hyokeun Park and Ahmet Yildiz for their instructions regarding the sample preparation. We thank Anna Li and Damien Garbett for protein preparation. This work was supported by National Institutes of Health Grants AR44420, AR48931 and GM68625 and National Science Foundation Grants DBI-02-15869 and 0134916.

References

1. Berg, J. S., B. C. Powell, and R. E. Cheney. 2001. A millennial myosin census. Mol Biol Cell 12:780-794.

2. Kellerman, K. A. and K. G. Miller. 1992. An unconventional myosin heavy chain gene from Drosophila melanogaster. J Cell Biol 119:823-834.

3. Hasson, T. and M. S. Mooseker. 1994. Porcine myosin-VI: characterization of a new mammalian unconventional myosin. J Cell Biol 127:425-440.

4. Avraham, K. B., T. Hasson, T. Sobe, B. Balsara, J. R. Testa, A. B. Skvorak, C. C. Morton, N. G. Copeland, and N. A. Jenkins. 1997. Characterization of unconventional MYO6, the human homologue of the gene responsible for deafness in Snell's waltzer mice. Hum Mol Genet 6:1225-1231.

5. Avraham, K. B., T. Hasson, K. P. Steel, D. M. Kingsley, L. B. Russell, M. S. Mooseker, N. G. Copeland, and N. A. Jenkins. 1995. The mouse Snell's waltzer deafness gene encodes an unconventional myosin required for structural integrity of inner ear hair cells. Nat Genet 11:369-375.

6. Hasson, T., P. G. Gillespie, J. A. Garcia, R. B. MacDonald, Y. Zhao, A. G. Yee, M. S. Mooseker, and D. P. Corey. 1997. Unconventional myosins in inner-ear sensory epithelia. J Cell Biol 137:1287-1307.

7. Wells, A. L., A. W. Lin, L. Q. Chen, D. Safer, S. M. Cain, T. Hasson, B. O. Carragher, R. A. Milligan, and H. L. Sweeney. 1999. Myosin VI is an actin-based motor that moves backwards. Nature 401:505-508.

8. Buss, F., S. D. Arden, M. Lindsay, J. P. Luzio, and J. Kendrick-Jones. 2001. Myosin VI isoform localized to clathrin-coated vesicles with a role in clathrin-mediated endocytosis. Embo J 20:3676-3684.

9. Aschenbrenner, L., T. Lee, and T. Hasson. 2003. Myo6 facilitates the translocation of endocytic vesicles from cell peripheries. Mol Biol Cell 14:2728-2743.

10. Lister, I., S. Schmitz, M. Walker, J. Trinick, F. Buss, C. Veigel, and J. Kendrick-Jones. 2004. A monomeric myosin VI with a large working stroke. Embo J 23:1729-1738.

11. Rock, R. S., S. E. Rice, A. L. Wells, T. J. Purcell, J. A. Spudich, and H. L. Sweeney. 2001. Myosin VI is a processive motor with a large step size. Proc Natl Acad Sci U S A 98:13655-13659.

12. Nishikawa, S., K. Homma, Y. Komori, M. Iwaki, T. Wazawa, A. Hikikoshi Iwane, J. Saito, R. Ikebe, E. Katayama, T. Yanagida, and M. Ikebe. 2002. Class VI myosin moves processively along actin filaments backward with large steps. Biochem Biophys Res Commun 290:311-317.

13. Yildiz, A., H. Park, D. Safer, Z. Yang, L. Q. Chen, P. R. Selvin, and H. L. Sweeney. 2004. Myosin VI Steps via a Hand-over-Hand Mechanism with Its Lever Arm Undergoing Fluctuations when Attached to Actin. J Biol Chem 279:37223-37226.

14. Okten, Z., L. S. Churchman, R. S. Rock, and J. A. Spudich. 2004. Myosin VI walks hand-over-hand along actin. Nat Struct Mol Biol 11(9)::884-887.

15. Altman, D., H. L. Sweeney, and J. A. Spudich. 2004. The mechanism of myosin VI translocation and its load-induced anchoring. Cell 116:737-749.

16. Mehta, A. D., R. S. Rock, M. Rief, J. A. Spudich, M. S. Mooseker, and R. E. Cheney. 1999. Myosin-V is a processive actin-based motor. Nature 400:590-593.

17. Yildiz, A., M. Tomishige, R. D. Vale, and P. R. Selvin. 2004. Kinesin Walks Hand-Over-Hand. Science 303:676-678.

18. Yildiz, A., J. N. Forkey, S. A. McKinney, T. Ha, Y. E. Goldman, and P. R. Selvin. 2003. Myosin V walks hand-over-hand: single fluorophore imaging with 1.5-nm localization. Science 300:2061-2065.

19. Sakamoto, T., I. Amitani, E. Yokota, and T. Ando. 2000. Direct observation of processive movement by individual myosin V molecules. Biochem Biophys Res Commun 272:586-590.

20. Purcell, T. J., C. Morris, J. A. Spudich, and H. L. Sweeney. 2002. Role of the lever arm in the processive stepping of myosin V. Proc Natl Acad Sci U S A 99:14159-14164.

21. Mehta, A. 2001. Myosin learns to walk. J Cell Sci 114:1981-1998.

22. Veigel, C., F. Wang, M. L. Bartoo, J. R. Sellers, and J. E. Molloy. 2002. The gated gait of the processive molecular motor, myosin V. Nat Cell Biol 4:59-65.

23. Forkey, J. N., M. E. Quinlan, M. A. Shaw, J. E. Corrie, and Y. E. Goldman. 2003. Three-dimensional structural dynamics of myosin V by single-molecule fluorescence polarization. Nature 422:399-404.

24. Warshaw, D. M., G. Kennedy, S. Work, E. Krementsova, S. Beck, and K. Trybus. 2005. Differential Labeling of Myosin V Heads with Quantum Dots Allows Direct Visualization of Hand-Over-Hand Processivity. Biophys J 88:L30-L32.

25. Rock, R. S., B. Ramamurthy, A. R. Dunn, S. Beccafico, B. R. Rami, C. Morris, B. J. Spink, C. Franzini-Armstrong, J. A. Spudich, and H. L. Sweeney. 2005. A flexible domain is essential for the large step size and processivity of myosin VI. Mol Cell 17:603-609.

26. Gordon, M. P., T. Ha, and P. R. Selvin. 2004. Single-molecule high-resolution imaging with photobleaching. Proc Natl Acad Sci U S A 101:6462-6465.

27. Qu, X., D. Wu, L. Mets, and N. F. Scherer. 2004. Nanometer-localized multiple single-molecule fluorescence microscopy. PNAS:0402155101.

Figure Legends

Fig. 1. (a) Hand-over-hand mechanism of walking. (b) An alternative model of motility in which the separation between the myosin heads alternates between x and 60-x nm, while each head takes 60 nm steps sequentially. Cryo-electron microscopy images suggest that x could be much less than 30 nm.

Fig. 2. (a) Peak intensity versus time for a myosin VI dimer labeled with two eGFP's. (b) Pre and post photobleach of one of the eGFP's. The last graph shows the difference between the first two, which is the emission from the eGFP that photobleached first.

Fig.3. Histogram of measured separations between the myosin VI heads and three Gaussian fits to the data. The blue curve is a single Gaussian fit representing the hand-over-hand model, the black curve is an unconstraint fit of two Gaussians, and the red curve is fit of two Gaussians with constraints.

Figure 1

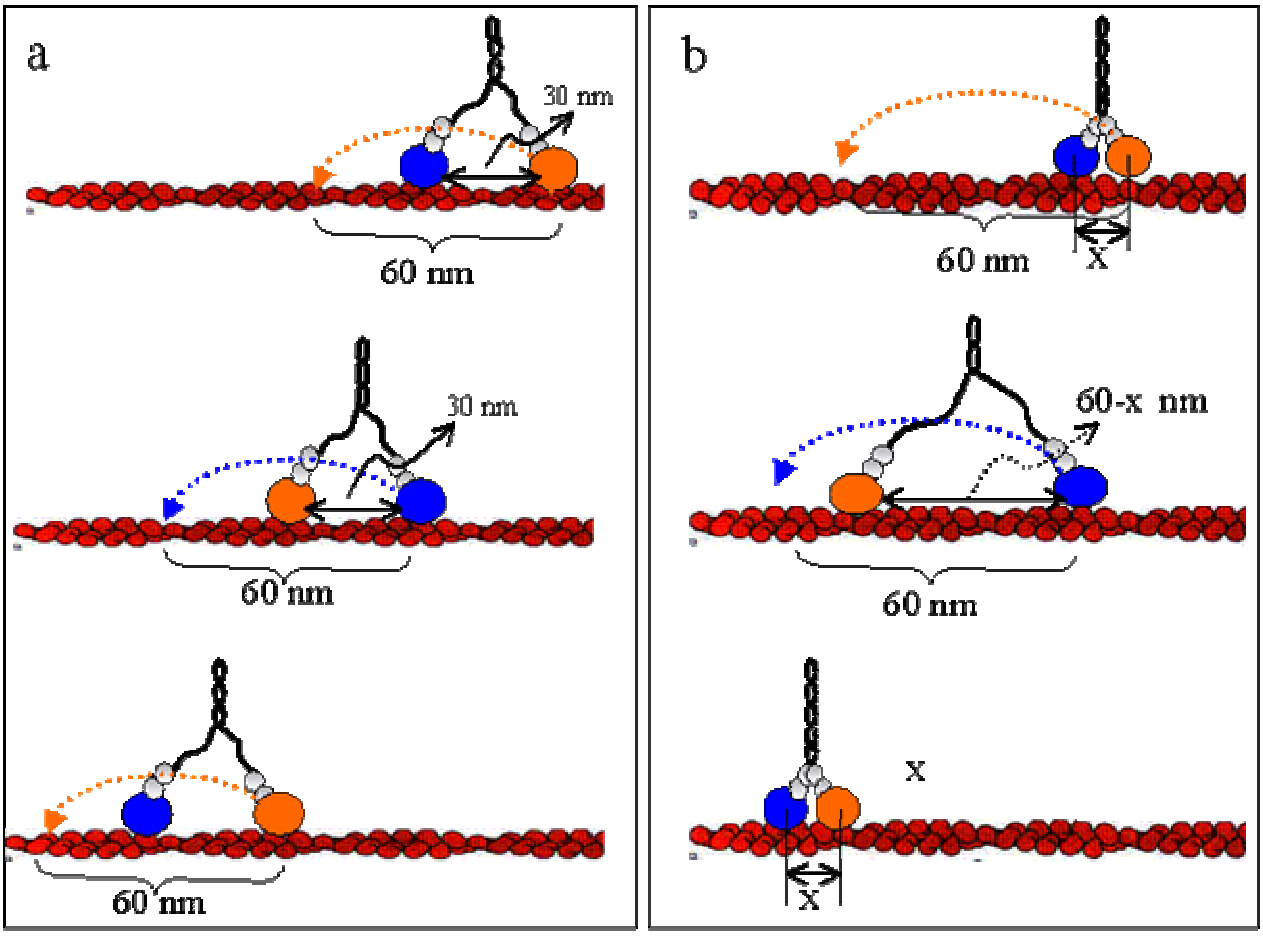

Figure 2

a

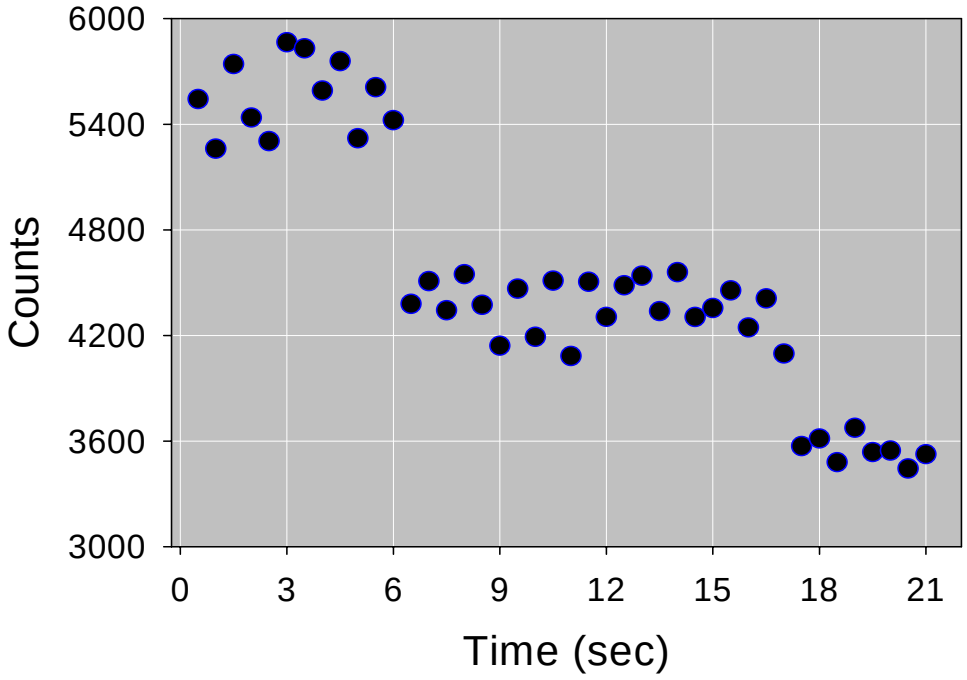
6000
5400
4800
4200
3600
3000
Counts
0
3
6
9
12
15
18
21
Time (sec)

b

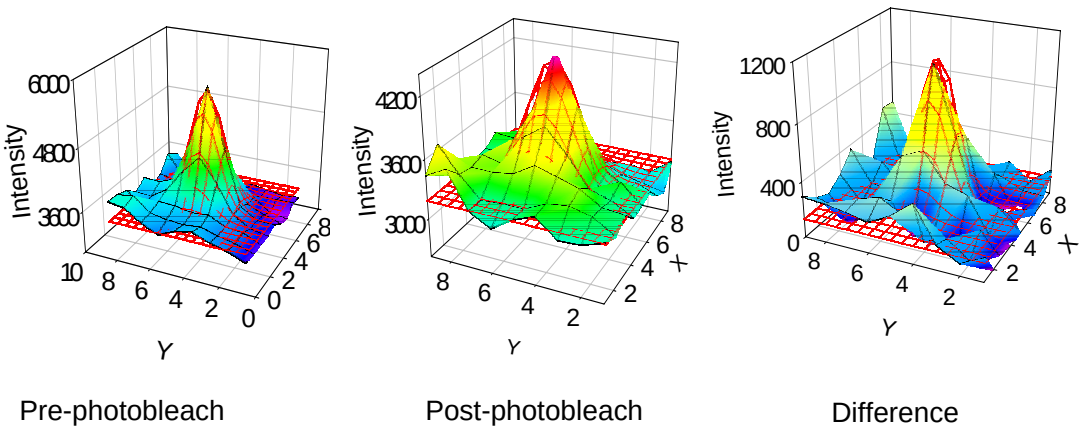
Intensity
6000
4800
3600
10
8
6
4
2
0
Y
0
2
4
6
8
Pre-photobleach
Intensity
4200
3600
3000
8
6
4
2
Y
2
4
6
8
X
Post-photobleach
Intensity
1200
800
400
0
8
6
4
2
Y
2
4
6
8
X
Difference

Figure 3

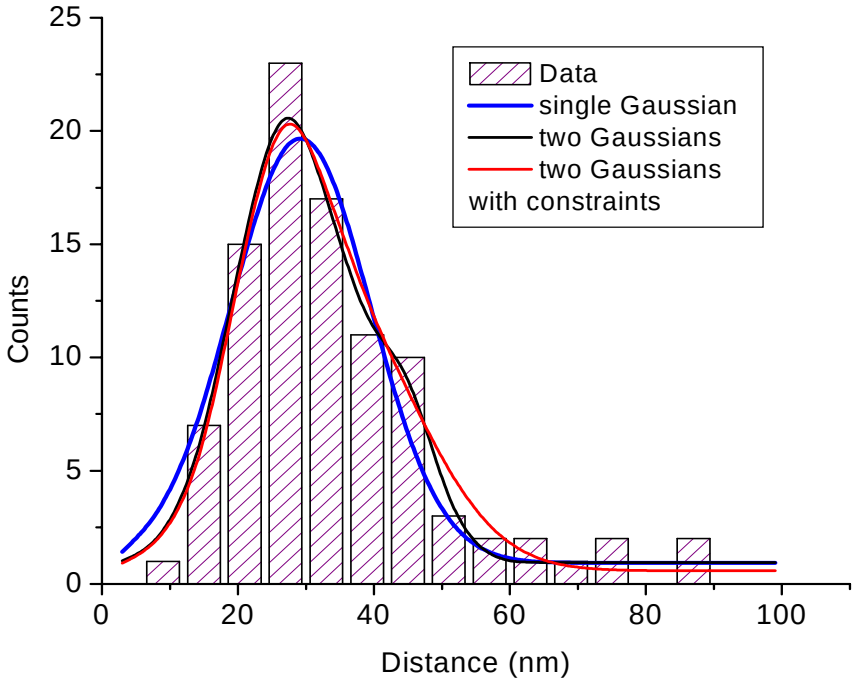
Data
single Gaussian
two Gaussians
two Gaussians
with constraints
Counts
Distance (nm)
0
5
10
15
20
25
0
20
40
60
80
100